

Marian Hebenbrock and Jens Müller*

1*H*-[1,2,4]Triazolo[4,3-*a*]pyridin-4-ium and 3*H*-[1,2,4]triazolo[4,3-*a*]quinolin-10-ium derivatives as new intercalating agents for DNA

<https://doi.org/10.1515/znb-2018-0089>

Received May 11, 2018; accepted May 13, 2018

Abstract: Two new cationic DNA intercalators, 3-phenyl-1-(6-phenylpyridin-2-yl)-1*H*-[1,2,4]triazolo[4,3-*a*]pyridin-4-ium (**1a**)⁺ and 1-phenyl-3-(6-phenylpyridin-2-yl)-3*H*-[1,2,4]triazolo[4,3-*a*]quinolin-10-ium (**1b**)⁺, were synthesized from 2-chloropyridine and 2-chloroquinoline, respectively, in a four-step procedure. Generation of the hydrazine, followed by condensation with an aldehyde to give a hydrazone and subsequent Buchwald-Hartwig amination gave a mixture of *E*- and *Z*-configured *N,N*-functionalized hydrazones. Finally, oxidative cyclisation gave rise to the formation of the cationic DNA intercalators, whose molecular structures were determined by single-crystal X-ray diffraction analysis of the hexafluorophosphate and tribromide salt of (**1a**)⁺ and (**1b**)⁺, respectively. The intercalative binding of (**1a**)PF₆ and (**1b**)PF₆ to ctDNA was confirmed by means of UV, CD and luminescence spectroscopy, determination of the DNA melting temperature and by rheology measurements.

Keywords: DNA; intercalator.

Dedicated to: Professor Werner Uhl on the occasion of his 65th birthday.

1 Introduction

Molecules capable of interacting with DNA may interfere with the regulation of gene expression and transcription. Hence, they are of interest due to their possible clinical relevance. In particular, non-covalently bound molecules have been extensively investigated. They are typically classified according to their DNA binding mode. The most common

non-covalent binding modes are groove binding, electrostatic interaction and intercalation [1]. Intercalation was first observed for acridine derivatives [2] and later found for many other small molecules, too, including metal complexes [3]. A comparison of efficient intercalators allows to delineate the following characteristics [4–7]: (1) a large aromatic π system, often involving three or more annulated aromatic rings, to guarantee an optimal stacking interaction with neighboring nucleobases; (2) a delocalized positive charge, to enable an attractive electrostatic interaction with the polyanionic nucleic acid; (3) the presence of additional external substituents, capable of interacting with the DNA *via* van der Waals interactions or *via* hydrogen bonding. Nowadays, ethidium bromide is one of the most commonly used intercalators in biochemical studies [8]. It belongs to the class of phenanthridine-derived intercalators [9]. We describe here the synthesis and characterization of two new intercalators mimicking structural characteristics of ethidium bromide, albeit not being phenanthridine derivatives (Chart 1). Common characteristics are the endocyclic iminium ion, the delocalized positive charge, and a phenyl substituent in *ortho* position to the iminium nitrogen atom.

2 Results and discussion

2.1 Synthesis

The synthesis of the new intercalators (**1a**)⁺ and (**1b**)⁺ started from 2-chloropyridine and 2-chloroquinoline, respectively (Scheme 1). Reaction with hydrazine monohydrate yielded the respective hydrazine derivatives **2a** and **2b** in a nucleophilic aromatic substitution, followed by a condensation reaction with benzaldehyde to give the hydrazones **3a** and **3b**. Next, reaction with *in-situ* generated 2-bromo-6-phenylpyridine resulted in the formation of *E*- and *Z*-configured **4a** and **4b** in a Buchwald-Hartwig amination (*E/Z* ratio: ca. 80/20). Temperature-dependent ¹H NMR spectroscopy did not indicate any equilibration between the isomers. Finally, reaction with bromine led to an oxidative cyclization, giving (**1a**)⁺ and (**1b**)⁺. As this oxidative cyclization involving the hydrazone carbon atom

*Corresponding author: Jens Müller, Westfälische Wilhelms-Universität Münster, Institut für Anorganische und Analytische Chemie, Corrensstraße 28/30, 48149 Münster, Germany, Phone: +49 251 83 36006, E-mail: mueller.j@uni-muenster.de

Marian Hebenbrock: Westfälische Wilhelms-Universität Münster, Institut für Anorganische und Analytische Chemie, Corrensstraße 28/30, 48149 Münster, Germany

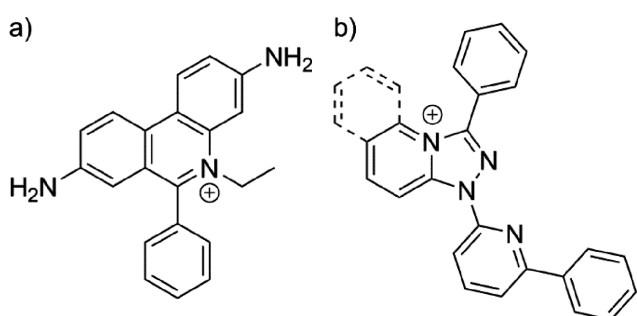


Chart 1: Structural representation of (a) ethidium and (b) 3-phenyl-1-(6-phenylpyridin-2-yl)-1H-[1,2,4]triazolo[4,3-a]pyridin-4-ium ((**1a**)⁺, solid lines only) and 1-phenyl-3-(6-phenylpyridin-2-yl)-3H-[1,2,4]triazolo[4,3-a]quinolin-10-ium cations ((**1b**)⁺, including dotted lines).

leads to a loss of the stereochemical information at the double bond, an interconversion of the *E*- and *Z*-isomers of **4a** and **4b** was not further investigated. The cationic intercalators were isolated as their hexafluorophosphate salts (**1a**)PF₆ and (**1b**)PF₆.

2.2 Structural characterization

The Buchwald-Hartwig amination product *E*-**4a** was obtained in the form of single crystals suitable for structure determination by X-ray diffraction analysis. Figure 1 shows the molecular structure of compound *E*-**4a**. The pyridyl moiety (ring A) is oriented almost perpendicularly

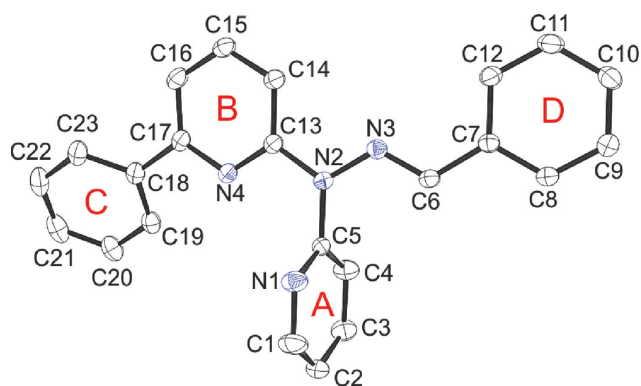
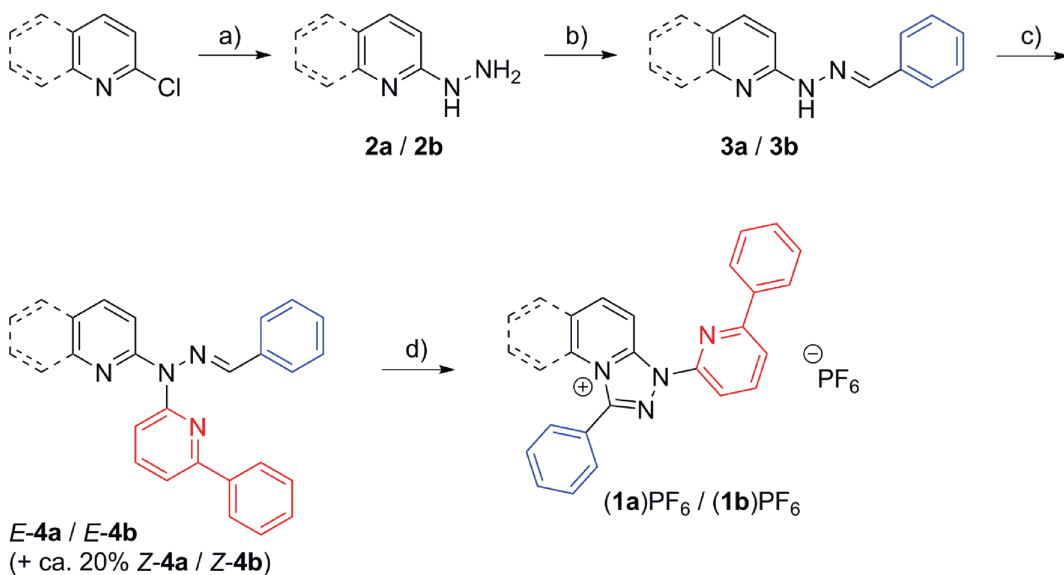


Fig. 1: Molecular structure of *E*-**4a** in the crystal. Displacement ellipsoids are drawn at the 30% probability level, H atoms are omitted for clarity. Letters A–D represent the planes of the respective aromatic rings.

with respect to the hydrazone (ring D). This contrasts the almost planar alignment found for closely related compounds bearing a methyl substituent at N2 rather than a phenylpyridyl group [10]. The N2–C5 bond length of 1.438(2) Å is in agreement with this finding and indicates a lack of conjugation, in particular when compared with the N2–C13 bond length of 1.398(2) Å. In general, the bond lengths and angles in compound *E*-**4a** are in the expected range reported for related organic molecules [11].

The molecular structures of intercalators (**1a**)⁺ and (**1b**)⁺ were determined by single-crystal X-ray diffraction analysis, too. In the case of (**1b**)⁺, a crystal of the intermediate



Scheme 1: Synthesis of (**1a**)PF₆ and (**1b**)PF₆ from 2-chloropyridine (solid lines only) and 2-chloroquinoline (including dotted lines), respectively. (a) 7.3 equiv. N₂H₄ · H₂O, 120°C, 8 h; (b) 1.1 equiv. benzaldehyde, ethanol, 55°C, 1 h; (c) 1.5 equiv. 2-bromo-6-phenylpyridine, 5 mol% [1,1'-bis(diphenylphosphino)ferrocene]dichloridopalladium(II), 1.2 equiv. Cs₂CO₃, toluene, 100°C, 18 h; (d) 1. 6.4 equiv. Br₂, CH₃COOH, r. t., 1 h; 2. 3.5 equiv. KPF₆, acetone, 60°C, 6 h.

product $(\mathbf{1b})\text{Br}_3$ was obtained prior to the anion exchange to hexafluorophosphate. Intercalator $(\mathbf{1a})^+$ crystallized as the final product $(\mathbf{1a})\text{PF}_6^-$. Figure 2 shows the molecular structures of the respective cations. Table 1 lists relevant angles determined for $(\mathbf{1a})^+$ and $(\mathbf{1b})^+$ and compares them with those observed for compound *E-4a*. The data indicate that the cyclisation reaction essentially brings the pyridyl and quinolinyl substituents involving N1 (ring A) into the plane of the pyridyl moiety involving N4 (ring B). The quinoline-derived cation $(\mathbf{1b})^+$ is planarized to a larger extent than the pyridine-derived compound $(\mathbf{1a})^+$. For both intercalators, the phenyl substituent (ring D) is significantly out of plane, similar to what is known for the ethidium cation, where the dihedral angle amounts to 97°

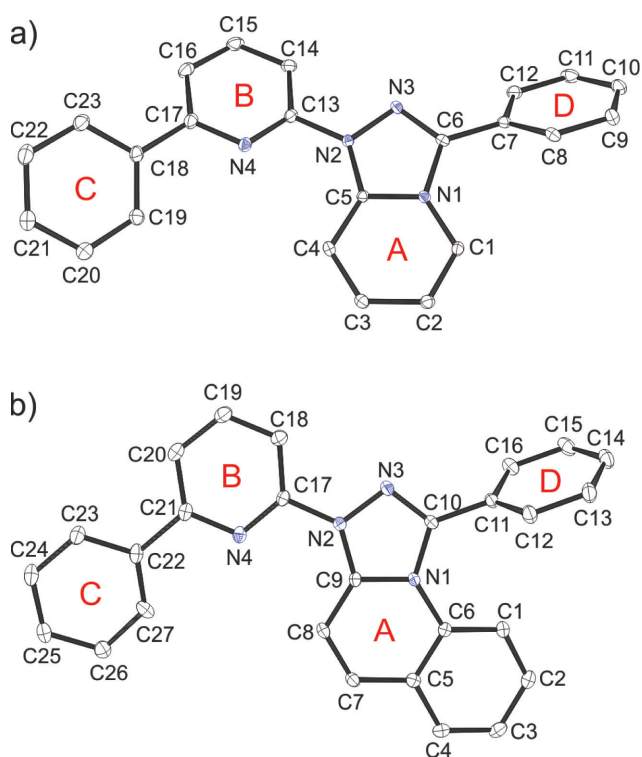


Fig. 2: Molecular structures of the cations of (a) $(\mathbf{1a})\text{PF}_6^-$ and (b) $(\mathbf{1b})\text{Br}_3$ in the crystal. Displacement ellipsoids are drawn at the 30% probability level, H atoms are omitted for clarity. Letters A–D represent the planes of the respective aromatic rings.

Table 1: Angles (deg) between the planes of the respective aromatic rings.

Ring planes	$(\mathbf{1a})^+$	$(\mathbf{1b})^+$	<i>E-4a</i>
A–B	16.02(8)	5.00(6)	85.1(1)
A–C	30.07(8)	6.82(6)	74.6(1)
A–D	44.41(8)	69.05(7)	72.8(1)
B–C	31.9(1)	10.64(8)	28.3(1)

[12]. The larger angle observed for $(\mathbf{1b})^+$ compared to $(\mathbf{1a})^+$ may be due to a different extent of repulsion of the hydrogen atom at carbon atom C1 and those attached to ring D.

2.3 Characterization of the intercalators

To investigate the intercalating capability of $(\mathbf{1a})\text{PF}_6^-$ and $(\mathbf{1b})\text{PF}_6^-$, a series of experiments were performed. Initially, a solution of calf thymus DNA (ctDNA) was titrated with increasing amounts of the intercalators. For both complexes, a more or less constant increase in absorbance was observed (data not shown), which can be directly correlated to the increasing concentrations. Based on these data, a conclusion on a possible interaction of ctDNA and $(\mathbf{1a})^+$ or $(\mathbf{1b})^+$ is not possible. Consequently, the reverse experiment was performed, too. As can be seen from Fig. 3, significant changes in the absorbance of the cations can be observed upon the stepwise addition of ctDNA. Of particular importance is the hypochromicity at wavelengths >300 nm, accompanied by a bathochromic shift by 10 nm of the absorbance maximum ($321 \rightarrow 331$ nm for $(\mathbf{1a})^+$, $334 \rightarrow 344$ nm for $(\mathbf{1b})^+$). Such hypochromic effects in combination with a bathochromic shift are considered strong indicators for an intercalative process [4]. Isosbestic points at 296 and 344 nm for $(\mathbf{1a})^+$ and at 290 and 354 nm for $(\mathbf{1b})^+$ confirm a two-state equilibrium process for the adduct formation between DNA and intercalator.

In addition, circular dichroism (CD) spectroscopy was applied to characterize further the DNA-binding properties of the intercalators. Prior to the addition of $(\mathbf{1a})^+$ or $(\mathbf{1b})^+$, the CD spectrum of ctDNA resembles that of canonical B-DNA (Fig. 4) [13], displaying Cotton effects at 245 (negative) and 277 nm (positive). Upon titrating the ctDNA solution with the intercalators, a small bathochromic shift of the negative Cotton effect is observed. Nonetheless, the CD spectra in the presence of $(\mathbf{1a})^+$ or $(\mathbf{1b})^+$ still indicate the presence of a canonical right-handed helix, as is expected for an intercalative process. Of particular interest is the induced circular dichroism at 325 (for $(\mathbf{1a})^+$) and 336 nm (for $(\mathbf{1b})^+$) (Fig. 4). An induced circular dichroism occurs when an achiral molecule (such as the intercalators investigated in this study) tightly binds to a chiral molecule (such as the DNA helices), so that it experiences a constant chiral environment. Such an effect is well-known for DNA-binding molecules [14]. Intercalators are characterized by a negative induced Cotton effect [15]. Hence, the CD spectra shown in Fig. 4 provide further experimental proof for an intercalative action of $(\mathbf{1a})^+$ and $(\mathbf{1b})^+$.

The CD data can be used to determine the number of intercalators per duplex, as the change in molar ellipticity

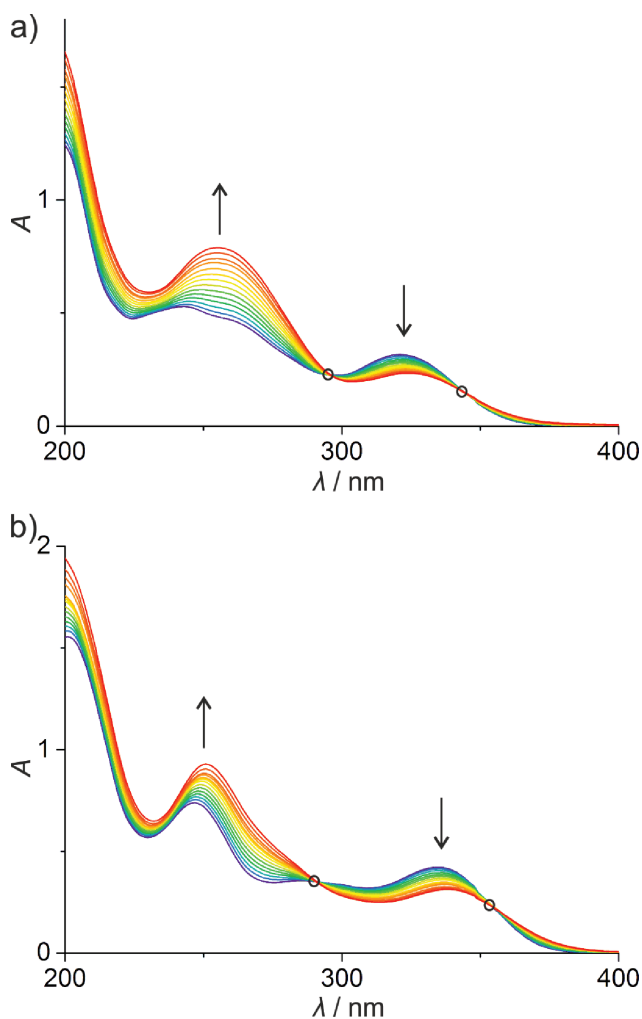


Fig. 3: UV spectra of (a) **(1a)**PF₆ and (b) **(1b)**PF₆ (2.4×10^{-5} M in Tris · HCl buffer, pH 7.4) upon stepwise addition of ctDNA (11 steps with an increase of 6.1×10^{-6} M each). Arrows indicate the directions of changes, circles represent isosbestic points.

at a wavelength attributed to a ctDNA-based transition should correlate with the number of bound molecules. Figure 5 shows plots of the molar ellipticity at the wavelengths of the Cotton effects depending on the amount of **(1a)**⁺ and **(1b)**⁺ present in solution. For **(1a)**⁺, the molar ellipticity increases linearly until approximately 0.25 equivalents of intercalator are present per nucleotide. The addition of more **(1a)**⁺ does not lead to any further changes. This ratio of one intercalator per two base pairs agrees well with the nearest-neighbor exclusion principle established for DNA intercalators [16]. The same ratio is also observed for **(1b)**⁺, where the experimental data would also be in agreement with a somewhat lower occupancy.

An intercalative binding is typically accompanied by an increase in the DNA melting temperature of at least 5–8°C [17]. Hence, the melting temperature of ctDNA was

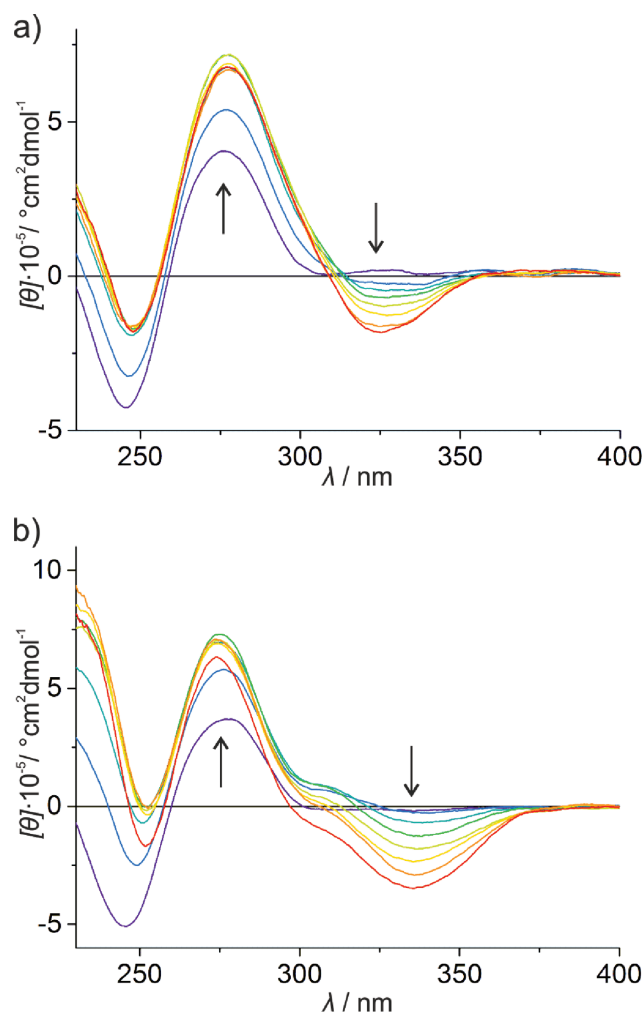


Fig. 4: CD spectra of ctDNA (7.6×10^{-5} M in Tris · HCl buffer, pH 7.4) upon stepwise addition of (a) **(1a)**PF₆ and (b) **(1b)**PF₆ (seven steps with an increase of 7.9×10^{-6} M each). Arrows indicate the directions of changes.

determined in the absence and presence of **(1a)**⁺ and **(1b)**⁺. Two complementary approaches were used in this respect, namely temperature-dependent UV and CD spectroscopy. As can be seen from the data summarized in Table 2, both methodologies clearly indicate a significant increase in T_m upon the addition of **(1a)**⁺ or **(1b)**⁺, again supporting their intercalative action. The values of T_m and ΔT_m appear to depend on which method is used for their determination. This can be explained in two ways. (1) The melting temperature determined by temperature-dependent UV spectroscopy $T_{m,UV}$ indicates a loss of base stacking, whereas $T_{m,CD}$ relates to a loss of helicity. As these two phenomena do not necessarily occur at the same temperature, differences between $T_{m,UV}$ and $T_{m,CD}$ are not unexpected. (2) The intercalators may also display a temperature-dependent UV absorbance. As $T_{m,UV}$ is determined by monitoring the

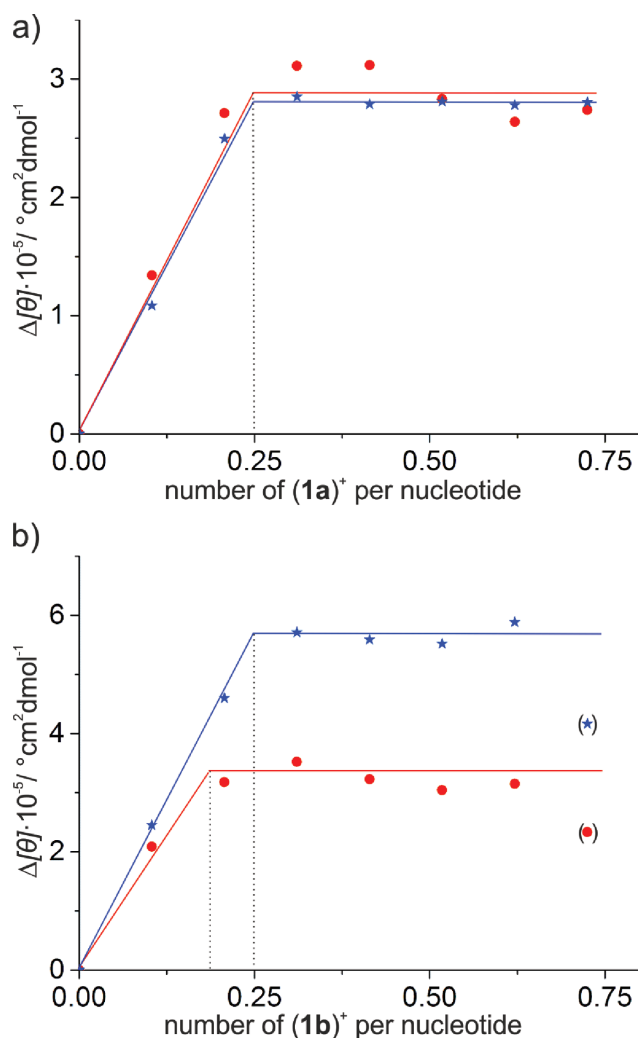


Fig. 5: Change of molar ellipticity of ctDNA (7.6×10^{-5} M in Tris · HCl buffer, pH 7.4) upon stepwise addition of (a) $(1a)PF_6$ (★: 245 nm, ●: 277 nm) and (b) $(1b)PF_6$ (★: 248 nm, ●: 277 nm). Data points in parentheses have not been included in the fit.

Table 2: Melting temperature T_m (°C) and change of the melting temperature ΔT_m (°C) of ctDNA in the presence of the intercalators, determined by temperature-dependent UV ($T_{m,UV}$) or CD ($T_{m,CD}$) spectroscopy.^a

	$T_{m,UV}^b$	$\Delta T_{m,UV}^b$	$T_{m,CD}^c$	$\Delta T_{m,CD}^c$
ctDNA	60		62	
ctDNA+(1a) ⁺	70	+10	75	+13
ctDNA+(1b) ⁺	74	+14	80	+18

^aExperimental conditions: 76 μM ctDNA, 24 μM intercalator, Tris · HCl buffer; ^bdetermined at 260 nm; ^cdetermined at 277 nm.

absorbance at 260 nm, the data obtained UV-spectroscopically are therefore potentially impacted by such an interference and are hence less reliable.

Luminescence spectroscopy was applied as another independent method to study the interaction of cations $(1a)^+$ and $(1b)^+$ with ctDNA. As can be seen from Fig. 6, a so-called light-switch effect occurs, which is well-known for DNA intercalators [4]. In the absence of any ctDNA, the luminescence of the intercalators is partially quenched. Addition of ctDNA immediately leads to an increase in luminescence by $\sim 100\%$. Larger amounts of ctDNA induce a gradual decline in luminescence intensity again, probably as a result of charge transfer processes within the DNA duplex [18].

Finally, the viscosity of ctDNA solutions containing DNA-interacting compounds is a good indicator for the mode of interaction. As an intercalating molecule essentially stretches the DNA duplex and leads to an increased hydrodynamic radius, intercalation is typically

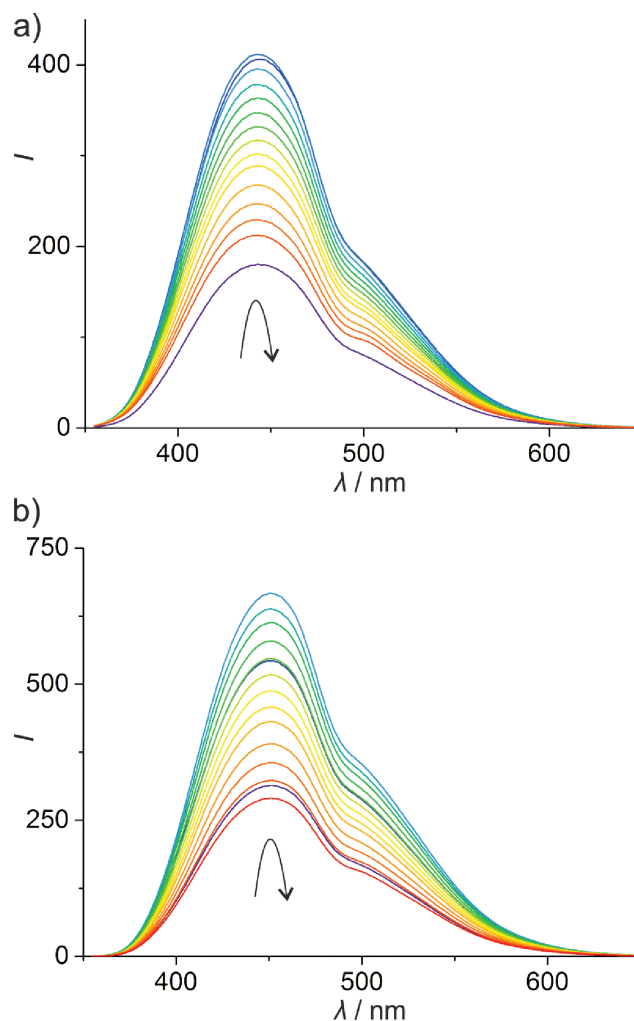


Fig. 6: Luminescence spectra of (a) $(1a)PF_6$ and (b) $(1b)PF_6$ (2.4×10^{-5} M in Tris · HCl buffer, pH 7.4) upon stepwise addition of ctDNA (13 steps with an increase of 8.1×10^{-6} M each).

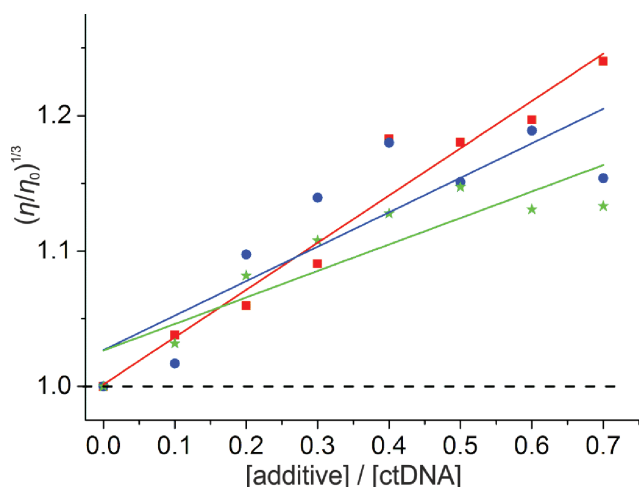


Fig. 7: Cohen-Eisenberg plot of the viscosity of **(1a)⁺** (■, red), **(1b)⁺** (●, blue) and ethidium bromide (★, green). Experimental conditions: 7.6×10^{-5} M ctDNA in Tris · HCl buffer (pH 7.4), stepwise addition of additive (seven steps with an increase of 7.9×10^{-6} M each).

accompanied by an increase in viscosity. In contrast, groove-binding compounds are known to not significantly influence the viscosity, as they merely bind to an existing void and hence do not induce relevant conformational changes [14]. Figure 7 shows how the relative viscosity changes upon the addition of the intercalators. In addition to **(1a)⁺** and **(1b)⁺**, ethidium bromide was investigated as a well-known intercalator. For all three compounds, a significant increase in viscosity was observed. In fact, intercalators **(1a)⁺** and **(1b)⁺** lead to an even steeper increase in relative viscosity than ethidium bromide. Hence, the viscosity measurements confirm the intercalative binding mode of **(1a)⁺** and **(1b)⁺**.

3 Summary

Two new intercalators were synthesized starting from 2-chloropyridine and 2-chloroquinoline, respectively. Various spectroscopic methods clearly indicate that the resulting triazolopyridinium and triazoloquinolinium cations **(1a)⁺** and **(1b)⁺** indeed bind to ctDNA in an intercalative binding mode. According to their molecular structures, a triazole-bound phenyl moiety is significantly tilted with respect to the triazole ring system. An analogous behavior is known for the established intercalator ethidium bromide. It can be anticipated that the tilted substituent serves as some type of anchor upon intercalation of the cation into the DNA base stack. The straightforward synthesis by means of hydrazone formation, Buchwald-Hartwig amination and oxidative cyclisation will allow an

easy access to a variety of structural variants of this new class of intercalators.

4 Experimental section

4.1 General

2-Hydrazinylpyridine (**2a**) and 2-hydrazinylquinoline (**2b**) were prepared according to literature procedures [19, 20]. The reactions were carried out under argon atmosphere with degassed reactants and solvents. NMR spectra were recorded using Bruker Avance(I) 400 and Bruker Avance(III) 400 spectrometers. Electrospray ionization (ESI MS) mass spectra were recorded on a Bruker Daltonics MicroT of with loop injection. Elemental analyses were performed on a Vario EL III CHNS instrument. Absorbance spectra (titrations) were recorded on a Varian Cary 100 Bio spectrometer (25°C, data interval 1 nm), CD spectra were recorded on JASCO J-815 (25°C, data interval 0.1 nm) and luminescence spectra were recorded on JASCO FP-6500 instruments (data interval 0.5 nm). In the latter case, the samples were excited at 335 nm (bandwidth 5 nm, PMT voltage 300 V).

4.2 Synthesis of 2-(2-benzylidenehydrazinyl)pyridine (**3a**)

Compound **2a** (219 mg, 2.01 mmol), benzaldehyde (215 μ L, 2.10 mmol, 1.05 equiv.) and acetic acid (80 μ L) were dissolved in ethanol (8 mL) and the mixture stirred for 1 h at 55°C. The solution was reduced to one third of its original volume. Water (1 mL) was added, and the solution was stored at 4°C overnight. The precipitate was washed with cold water and dried *in vacuo*. Compound **3a** (263 mg, 1.33 mmol, 66%) was isolated as a brownish solid. – ¹H NMR (400 MHz, CDCl₃, 27°C): δ = 9.37–9.02 (m, 1H, H7), 8.27–8.07 (m, 1H, H6), 7.79 (s, 1H, H9), 7.73–7.65 (m, 2H, H11), 7.65–7.59 (m, 1H, H4), 7.45–7.29 (m, 4H, H5, H12, H13), 6.83–6.74 (m, 1H, H3) ppm. – HRMS ((+)-ESI): m/z = 220.0851 (calcd. 220.0845 for [C₁₂H₁₁N₃Na]⁺). – Analysis for C₁₂H₁₁N₃ (%): calcd. C 73.1, H 5.6, N 21.3; found C 72.9, H 5.5, N 21.1.

4.3 Synthesis of 2-(2-benzylidene-1-(pyridin-2-yl)hydrazinyl)-6-phenylpyridine (**4a**)

Phenylboronic acid (325 mg, 2.67 mmol), 2,6-dibromopyridine (632 mg, 2.67 mmol, 1.0 equiv.), triphenylphosphane

(161 mg, 0.530 mmol, 0.2 equiv.) and K_2CO_3 (2.95 g, 21.4 mmol, 8.0 equiv.) were degassed in a solution of dimethoxyethane (17 mL) and water (17 mL). Following the addition of $Pd(OAc)_2$ (35 mg, 0.13 mmol, 0.05 equiv.), the solution was stirred for 1 d at 110°C. After extracting with CH_2Cl_2 , the combined organic layers were dried ($MgSO_4$) and the solvent removed *in vacuo*. The solid residue was filtered through Celite using Et_2O and the solvent removed *in vacuo*. The crude product was combined with compound **3a** (404 mg, 2.05 mmol, 0.8 equiv.), [1,1'-bis(diphenylphosphino)ferrocene]dichloridopalladium(II) (75 mg, 0.10 mmol, 0.04 equiv.) and Cs_2CO_3 (868 mg, 2.46 mmol, 0.9 equiv.) and the mixture dried *in vacuo* for 5 h. Following the addition of toluene (10 mL), the solution was stirred for 18 h at 100°C. The mixture was extracted with ethyl acetate, the combined organic layers dried ($MgSO_4$) and the solvent removed *in vacuo*. The crude product was purified by column chromatography (SiO_2 , ethyl acetate-cyclohexane, 20:1) to give compound **4a** as a yellowish solid (610 mg, 1.73 mmol, 65%). According to the 1H NMR data, a mixture of *E* and *Z* isomers was obtained (*E:Z* = 3.8:1.0). The assignment of the *E* and *Z* isomer was made in comparison with literature precedents [21, 22]. – 1H NMR (400 MHz, $CDCl_3$, 27°C, *E* isomer): δ = 8.52–8.44 (m, 1H, H6), 7.91–7.80 (m, 4H, H4, H18, H21), 7.72–7.49 (m, 6H, H3, H9, H11, H17, H19), 7.42–7.28 (m, 6H, H12, H13, H22, H23), 7.17–7.09 (m, 1H, H5) ppm. 1H NMR (400 MHz, $CDCl_3$, 27°C, *Z* isomer): δ = 8.60–8.54 (m, 1H, H6), 7.91–7.80 (m, 3H, H9, H21), 7.74–7.43 (m, 6H, H3, H11, H17, H18, H19), 7.42–7.28 (m, 7H, H4, H12, H13, H22, H23), 7.17–7.09 (m, 1H, H5) ppm. – ^{13}C NMR (101 MHz, $CDCl_3$, 27°C, *E* isomer): δ = 156.2 (C14), 155.4 (C2), 155.1 (C16), 148.8 (C6), 139.0 (C18), 138.8 (C20), 138.7 (C9), 138.1 (C4), 135.6 (C10), 128.9 (C23), 128.8 (C13), 128.5 (C12), 128.5 (C22), 126.7 (C11), 126.7 (C21), 119.8 (C5), 118.1 (C3), 116.1 (C17), 115.5 (C19) ppm. ^{15}N NMR (41 MHz, $CDCl_3$, 27°C, *E* isomer): δ = 326 (N8), 292 (N1), 285 (N15), 162 (N7) ppm. – HRMS ((+)-ESI): m/z = 351.1614 (calcd. 351.1610 for $[C_{23}H_{20}N_4]^+$). – Analysis for $C_{23}H_{19}N_4 \cdot 0.15 EtOAc \cdot 2.75 H_2O$ (%): calcd. C 68.8, H 6.0, N 13.6; found C 68.7, H 5.6, N 13.4.

4.4 Synthesis of 3-phenyl-1-(6-phenylpyridin-2-yl)-1*H*-[1,2,4]triazolo[4,3-*a*]pyridin-4-ium hexafluorophosphate ((**1a**)PF₆)

A solution of bromine (333 μ L, 6.50 mmol, 6.5 equiv.) in acetic acid (4 mL) was added dropwise at 30°C within 1 h to a solution of compound **4a** (350 mg, 1.00 mmol) in acetic acid (14 mL). Water (10 mL) was added, and the resulting precipitate was washed with water and acetonitrile. The solid was recrystallized from DMF overnight using

Et_2O as antisolvent. The crystalline solid was dissolved in acetone (10 mL) and stirred for 6 h at 60°C. Following the addition of KPF_6 (644 mg, 3.50 mmol, 3.5 equiv.), the solvent was removed *in vacuo*, and the solid residue was washed with water, ethanol and Et_2O . Compound (**1a**)PF₆ was isolated as a yellowish solid (391 mg, 0.790 mmol, 79%). – 1H NMR (400 MHz, $[D_6]DMSO$, 27°C): δ = 9.31–9.20 (m, 1H, H3), 9.19–9.08 (m, 1H, H6), 8.68–8.54 (m, 1H, H4), 8.41–8.15 (m, 5H, H17, H18, H19, H21), 8.13–8.01 (m, 2H, H11), 7.92–7.76 (m, 4H, H5, H12, H13), 7.72–7.53 (m, 3H, H22, H23) ppm. – ^{13}C NMR (101 MHz, $[D_6]DMSO$, 27°C): δ = 156.0 (C16), 149.6 (C14), 146.5 (C9), 142.1 (C2), 141.8 (C18), 141.1 (C4), 136.9 (C20), 132.7 (C13), 130.1 (C23), 129.7 (C11), 129.6 (C12), 129.2 (C22), 128.0 (C6), 126.9 (C21), 121.9 (C10), 120.9 (C17), 120.3 (C5), 114.0 (C3), 113.4 (C19) ppm. – ^{15}N NMR (41 MHz, $[D_6]DMSO$, 27°C): δ = 274 (N15), 201 (N7), 200 (N1) ppm. – HRMS ((+)-ESI): m/z = 349.1462 (calcd. 349.1448 for $[C_{23}H_{17}N_4]^+$).

4.5 Synthesis of 2-(2-benzylidenehydrazinyl)quinoline (3b)

Compound **3b** was synthesized in analogy to compound **3a**, starting from compound **2b** (463 mg, 2.91 mmol). The product was isolated as a brownish solid (591 mg, 2.39 mmol, 82%). – 1H NMR (400 MHz, $CDCl_3$, 27°C): δ = 10.35–9.00 (br, 1H, H11), 8.26–7.93 (m, 1H, H4), 7.93–7.49 (m, 7H, H3, H6, H8, H9, H13, H15), 7.45–7.18 (m, 4H, H7, H16, H17). – HRMS ((+)-ESI): m/z = 248.1179 (calcd. 248.1188 for $[C_{16}H_{14}N_3]^+$). – Analysis for $C_{16}H_{13}N_3$ (%): calcd. C 77.7, H 5.3, N 17.0; found C 77.3, H 5.2, N 16.8.

4.6 Synthesis of 2-(2-benzylidene-1-(6-phenylpyridin-2-yl)hydrazinyl)quinoline (4b)

Compound **4b** was synthesized in analogy to compound **4a**, using compound **3b** (507 mg, 2.05 mmol). The product was isolated as a yellowish solid (682 mg, 1.70 mmol, 64%). – 1H NMR (400 MHz, $CDCl_3$, 27°C, *E* isomer): δ = 8.25–8.19 (m, 1H, H4), 7.98–7.77 (m, 6H, H6, H13, H15, H25), 7.73–7.56 (m, 10H, H3, H4, H8, H9, H11, H16, H17, H26), 7.55–7.41 (m, 2H, H7, H27), 7.40–7.29 (m, 3H, H21, H22, H23) ppm. 1H NMR (400 MHz, $CDCl_3$, 27°C, *Z* isomer): δ = 8.30–8.25 (m, 1H, H4), 7.98–7.77 (m, 6H, H6, H13, H15, H25), 7.73–7.56 (m, 10H, H3, H4, H8, H9, H11, H16, H17, H26), 7.55–7.41 (m, 2H, H7, H27), 7.40–7.29 (m, 3H, H21, H22, H23) ppm. – HRMS ((+)-ESI): m/z = 401.1761 (calcd. 401.1766 for $[C_{27}H_{21}N_4]^+$).

Table 3: Crystallographic data and data collection and refinement details for compounds (1a)PF₆, (1b)Br₃ and 4a.

	(1a)PF ₆	(1b)Br ₃	4a
Empirical formula	C ₂₃ H ₁₇ F ₆ N ₄ P	C ₂₇ H ₁₉ Br ₃ N ₄	C ₂₃ H ₁₈ N ₄
Formula weight	494.38	639.19	350.41
Crystal system	Monoclinic	Monoclinic	Monoclinic
Space group	<i>P</i> ₂ ₁ / <i>c</i>	<i>P</i> ₂ ₁ / <i>n</i>	<i>P</i> ₂ ₁ / <i>c</i>
<i>a</i> , Å	10.3768(5)	7.3902(3)	9.2715(2)
<i>b</i> , Å	27.815(1)	16.0635(6)	9.7627(2)
<i>c</i> , Å	7.6491(4)	20.3161(7)	20.7665(4)
β, deg	107.500(2)	99.432(1)	95.685(1)
<i>V</i> , Å ³	2105.6(2)	2379.2(2)	1870.43(7)
<i>Z</i>	4	4	4
ρ _{calcd} ^a , g cm ⁻³	1.56	1.78	1.24
μ(MoKα), mm ⁻¹	0.2	5.1	0.6
Crystal size, mm ³	0.88 × 0.26 × 0.22	0.57 × 0.41 × 0.36	0.19 × 0.17 × 0.10
Temperature, K	100(2)	100(2)	173(2)
θ range, deg	2.18–31.00	2.40–30.12	4.28–76.38
<i>hkl</i> range	0:14, –38:0, –10:10	–10:10, –22:22, –28:28	–11:11, –12:11, –22:26
Total/unique data/ <i>R</i> _{int}	14255/6178/0.165	37394/6983/0.038	12282/3708/0.056
Observed data [<i>I</i> > 2 σ(<i>I</i>)]	4329	5918	2892
<i>N</i> _{ref} / <i>N</i> _{par}	6178/307	6983/307	3708/244
<i>R</i> ₁ / <i>wR</i> ₂ [<i>I</i> > 2 σ(<i>I</i>)] ^{a, b}	0.0878/0.2318	0.0316/0.0773	0.0487/0.1193
<i>R</i> ₁ / <i>wR</i> ₂ (all data) ^{a, b}	0.1452/0.2633	0.0419/0.0814	0.0605/0.1302
<i>S</i> ^c	1.120	1.006	1.046
Min./max. res. dens., e Å ⁻³	1.50/–1.58	1.69/–0.50	0.20/–0.26

^a*R*₁ = Σ||*F*_o|| – ||*F*_c|| / Σ||*F*_o||; ^b*wR*₂ = [Σ*w*(*F*_o² – *F*_c²)² / Σ*w*(*F*_o²)^{1/2}]^{1/2}; ^c*S* = [σ²(*F*_o²) + (*AP*)² + (*BP*)²]⁻¹, where *P* = (Max(*F*_o², 0) + 2*F*_c²)/3; ^c*S* = GoF = [Σ*w*(*F*_o² – *F*_c²)² / (n_{obs} – n_{param})]^{1/2}.

4.7 Synthesis of 1-phenyl-3-(6-phenylpyridin-2-yl)-3H-[1,2,4]triazolo[4,3-*a*]quinolin-10-ium hexafluorophosphate ((1b)PF₆)

Compound (1b)PF₆ was synthesized in analogy to compound (1a)PF₆, starting from compound 4b (250 mg, 0.620 mmol). The product was isolated as a brownish solid (178 mg, 0.330 mmol, 53%). – ¹H NMR (400 MHz, [D₆]DMSO, 27°C): δ = 9.17 (d, *J* = 9.8 Hz, 1H, H3), 9.01 (d, *J* = 9.8 Hz, 1H, H4), 8.50–8.42 (m, 1H, H6), 8.42–8.24 (m, 4H, H21, H22, H25), 8.20–8.12 (m, 1H, 23), 8.01–7.82 (m, 7H, H7, H8, H15, H16, H17), 7.71–7.58 (m, 3H, H26, H27), 7.57–7.50 (m, 1H, H9) ppm. – ¹³C NMR (101 MHz, [D₆]DMSO, 27°C): δ = 156.1 (C20), 149.1 (C18), 148.2 (C13), 142.7 (C2), 142.2 (C4), 142.0 (C22), 136.7 (C24), 132.9 (C8), 132.7 (C17), 130.8 (C6), 130.5 (C10), 130.2 (C27), 130.1 (C15), 129.8 (C16), 129.2 (C26), 128.9 (C7), 126.9 (C25), 125.3 (C14), 124.9 (C5), 121.6 (C21), 116.6 (C9), 114.6 (C23), 110.6 (C3) ppm. – ¹⁵N NMR (41 MHz, [D₆]DMSO, 27°C): δ = 276 (N19), 205 (N11), 188 (N1) ppm. – HRMS ((+)-ESI): *m/z* = 399.1620 (calcd. 399.1604 for [C₂₇H₁₉N₄]⁺).

4.8 Crystal structure determinations

Single-crystal X-ray diffraction data were collected with graphite-monochromated MoKα radiation (λ = 0.71073 Å)

on a Bruker D8 Venture diffractometer. The structures were solved by Direct Methods and refined by full-matrix least-squares on *F*² by using the SHELXTL and SHELXL-97 programs [23]. Relevant crystallographic data are listed in Table 3.

CCDC 1842465–1842467 contain the supplementary crystallographic data for this paper. These data can be obtained free of charge from The Cambridge Crystallographic Data Centre via www.ccdc.cam.ac.uk/data_request/cif.

References

- [1] A. A. Almaqwashi, T. Paramanathan, I. Rouzina, M. C. Williams, *Nucleic Acids Res.* **2016**, *44*, 3971.
- [2] L. S. Lerman, *J. Mol. Biol.* **1961**, *3*, 18.
- [3] K. W. Jennette, S. J. Lippard, G. A. Vassiliades, W. R. Bauer, *Proc. Natl. Acad. Sci. USA* **1974**, *71*, 3839.
- [4] B. M. Zeglis, V. C. Pierre, J. K. Barton, *Chem. Commun.* **2007**, 4565.
- [5] A. S. Biebricher, I. Heller, R. F. H. Roijmans, T. P. Hoekstra, E. J. G. Peterman, G. J. L. Wuite, *Nat. Commun.* **2015**, *6*, 7304.
- [6] M. R. Gill, S. N. Harun, S. Halder, R. A. Boghazian, K. Ramadan, H. Ahmad, K. A. Vallis, *Sci. Rep.* **2016**, *6*, 31973.
- [7] N. W. Luedtke, J. S. Hwang, E. Nava, D. Gut, M. Kol, Y. Tor, *Nucleic Acids Res.* **2003**, *31*, 5732.
- [8] L.-M. Tumor, M. Radić Stojković, I. Piantanida, *Beilstein J. Org. Chem.* **2014**, *10*, 2930.

- [9] N. W. Luedtke, Q. Liu, Y. Tor, *Chem. Eur. J.* **2005**, *11*, 495.
- [10] A. Schmidt, M. Baune, A. Hepp, J. Kösters, J. Müller, *Z. Naturforsch.* **2016**, *71b*, 527.
- [11] F. H. Allen, O. Kennard, D. G. Watson, L. Brammer, A. G. Orpen, R. Taylor, *J. Chem. Soc., Perkin Trans.* **1987**, *2*, S1.
- [12] E. Subramanian, J. Trotter, C. E. Bugg, *J. Cryst. Mol. Struct.* **1971**, *1*, 3.
- [13] M. Vorlíčková, I. Kejnovská, K. Bednářová, D. Renčíuk, J. Kypr, *Chirality* **2012**, *24*, 691.
- [14] M. Hebenbrock, G. González-Abradelo, C. A. Strassert, J. Müller, *Z. Anorg. Allg. Chem.* **2018**, *644*, 671.
- [15] N. C. Garbett, P. A. Ragazzon, J. B. Chaires, *Nat. Protoc.* **2007**, *2*, 3166.
- [16] D. M. Crothers, *Biopolymers* **1968**, *6*, 575.
- [17] C. V. Kumar, R. S. Turner, E. H. Asuncion, *J. Photochem. Photobiol. A* **1993**, *74*, 231.
- [18] C. A. M. Seidel, A. Schulz, M. H. M. Sauer, *J. Phys. Chem.* **1996**, *100*, 5541.
- [19] N. M. Gandikota, R. S. Bolla, I. V. K. Viswanath, S. Bethi, *Asian J. Chem.* **2017**, *29*, 1920.
- [20] D. G. Calatayud, E. López-Torres, M. A. Mendiola, *Eur. J. Inorg. Chem.* **2013**, *2013*, 80.
- [21] E. L. Romero, R. F. D’Vries, F. Zuluaga, M. N. Chaur, *J. Braz. Chem. Soc.* **2015**, *26*, 1265.
- [22] S. M. Landge, E. Tkatchouk, D. Benítez, D. A. Lanfranchi, M. Elhabiri, W. A. Goddard III, I. Aprahamian, *J. Am. Chem. Soc.* **2011**, *133*, 9812.
- [23] G. M. Sheldrick, *Acta Crystallogr.* **2008**, *A64*, 112.

Graphical synopsis

Marian Hebenbrock and Jens Müller
**1*H*-[1,2,4]Triazolo[4,3-*a*]pyridin-4-ium and
3*H*-[1,2,4]triazolo[4,3-*a*]quinolin-10-ium
derivatives as new intercalating agents
for DNA**

<https://doi.org/10.1515/znb-2018-0089>
Z. Naturforsch. 2018; x(x)b: xxx–xxx

